Title
Role of canopy-scale photochemistry in modifying biogenic-atmosphere exchange of reactive terpene species: Results from the CELTIC field study

Journal
Journal of Geophysical Research, 110(D17)

ISSN
0148-0227

Authors
Stroud, Craig
Makar, Paul
Karl, Thomas
et al.

Publication Date
2005

DOI
10.1029/2005jd005775

Role of canopy-scale photochemistry in modifying biogenic-atmosphere exchange of reactive terpene species: Results from the CELTIC field study

Craig Stroud,[1,2] Paul Makar,[3] Thomas Karl,[1] Alex Guenther,[1] Chris Geron,[4] Andrew Turnipseed,[1] Eiko Nemitz,[1,5] Brad Baker,[6] Mark Potosnak,[1,7] and Jose D. Fuentes[8]

Received 12 January 2005; revised 8 May 2005; accepted 6 June 2005; published 13 September 2005.

[1] A one-dimensional canopy model was used to quantify the impact of photochemistry in modifying biosphere-atmosphere exchange of trace gases. Canopy escape efficiencies, defined as the fraction of emission that escapes into the well-mixed boundary layer, were calculated for reactive terpene species. The modeled processes of emission, photochemistry, diffusive transport, and deposition were highly constrained based on intensive observations collected in a Loblolly Pine plantation at Duke Forest, North Carolina, during the CELTIC field study. Canopy top fluxes for isoprene and α,β-pinene were not significantly altered by photochemistry as calculated escape efficiencies were greater than 0.90 for both species. β-caryophyllene emission and photochemistry were added to the canopy model as a surrogate for the reactive sesquiterpene class of species. β-caryopyllene escape efficiencies of 0.30 were calculated for midday summertime conditions. Urbanization scenarios were also performed to assess the impact of pollution on modifying biosphere-atmosphere exchange. Modest changes in escape efficiencies were calculated for a wide range of anthropogenic hydrocarbon and NO_x mixing ratios suggesting a simple parameterization of escape efficiency in terms of grid cell NO_x may be possible for incorporating the impact of canopy scale photochemistry within biogenic emission processing systems for regional air quality and climate models. The inferred magnitude of sesquiterpene ozonolysis reactions has important implications on both daytime and nighttime radical formation in the canopy.

Citation: Stroud, C., P. Makar, T. Karl, A. Guenther, C. Geron, A. Turnipseed, E. Nemitz, B. Baker, M. Potosnak, and J. D. Fuentes (2005), Role of canopy-scale photochemistry in modifying biogenic-atmosphere exchange of reactive terpene species: Results from the CELTIC field study, *J. Geophys. Res.*, *110*, D17303, doi:10.1029/2005JD005775.

1. Introduction

[2] Biogenic hydrocarbon emissions are estimated to be a larger source of reduced carbon to the global atmosphere than anthropogenic hydrocarbon emissions and are of comparable magnitude to the global emissions of methane [*Guenther et al.*, 1995]. The speciation and emission rate of biogenic hydrocarbons are highly variable depending on vegetation type, temperature, photosynthetically active radiation (PAR), atmospheric carbon dioxide (CO_2) levels, soil nutrient and water availability, among other factors [*Fuentes et al.*, 2000; *Monson*, 2002]. Biogenic hydrocarbons initially react in the atmosphere with hydroxyl radicals (OH), nitrate radicals (NO_3), and olefinic hydrocarbons can react with ozone (O_3). Biogenic hydrocarbons provide the fuel to drive the formation of organic peroxy radicals which in the presence of nitrogen oxides (NO_x) convert nitric oxide (NO) to nitrogen dioxide (NO_2) resulting in the formation of tropospheric O_3 [*Trainer et al.*, 1987; *Barket et al.*, 2004]. The hydrocarbon oxidation process also results in the formation of multi-functional products, such as organic acids, which result in the formation of secondary organic aerosol [*Griffin et al.*, 1999]. As a result, the atmospheric chemistry of biogenic hydrocarbons can play a fundamental role in influencing air quality and climate [*Chameides et al.*, 1988; *Monson and Holland*, 2001].

[3] Despite large uncertainties, recent evidence suggests that forests emit unknown reactive hydrocarbons not currently accounted for in biogenic emissions processing systems within air quality and climate models, in addition to the more commonly studied compounds such as isoprene

[1]National Center for Atmospheric Research, Boulder, Colorado, USA.
[2]Now at Meteorological Service of Canada, Toronto, Ontario, Canada.
[3]Meteorological Service of Canada, Toronto, Ontario, Canada.
[4]Environmental Protection Agency, Research Triangle Park, North Carolina, USA.
[5]Now at Centre for Ecology and Hydrology, Edinburgh, UK.
[6]South Dakota School of Mines and Technology, Rapid City, South Dakota, USA.
[7]Now at Desert Research Institute, Reno, Nevada, USA.
[8]Department of Environmental Sciences, University of Virginia, Charlottesville, Virginia, USA.

0148-0227/05/2005JD005775

and monoterpenes. In a northern Michigan forest, the direct measurement of total OH reactivity, which is the inverse of OH lifetime, was significantly greater than expected [*Di Carlo et al.*, 2004]. The missing OH reactivity increased with temperature with similar temperature dependence as terpene emission. *Di Carlo et al.* [2004] hypothesize that unknown reactive biogenic species, perhaps terpenes, provide the missing OH reactivity. In an earlier study, in the same Michigan forest, *Faloona et al.* [2001] observed an unexpected nocturnal OH source and a dependence of nocturnal OH and hydroperoxy radicals (HO_2) on O_3. *Faloona et al.* [2001] postulated that the missing OH source could be from the ozonolysis of reactive terpenes. In a Sierra Nevada pine forest, measurements of volatile organic compounds (VOCs) reveal large quantities of previously unreported oxidation products of reactive biogenic precursors [*Holzinger et al.*, 2004] assuming that the observed species were primarily produced by atmospheric oxidation as opposed to direct emission. The emissions of their biogenic precursors must be larger than the emission of total measured terpenes to account for the observed oxidation product mixing ratios; however, little is known about potential yields of these species. Also, in the same Sierra forest, significant non-stomatal O_3 deposition was observed [*Kurpius and Goldstein*, 2003] indicating that chemical O_3 losses could be more important than previously considered. In the laboratory, the ozonolysis of terpenes are known to produce the OH radical [*Paulson et al.*, 1998; *Aschmann et al.*, 2002]. Together these observations suggest that the ozonolysis of reactive terpenes may be a significant O_3 loss mechanism and OH source mechanism in the forest canopy. Recently, *Stroud et al.* [2002] also observed evidence for NO_3-initiated terpene oxidation just after sunset at an urban forested site in Nashville, TN. The NO_3-initiated oxidation of VOCs is another potential source for OH production. *Bey et al.* [2001] estimated that VOC + NO_3 reactions account for a maximum of 25% in OH production for conditions of high levels of biogenic compounds and moderate NO_x levels.

[4] The biogenic hydrocarbon emissions are first emitted into a forest canopy before some fraction, determined by the escape efficiency, is vented into the mixed boundary layer. The escape efficiency is defined as the ratio of the mass flux out of the canopy to the mass flux emitted within the canopy. In this study, the canopy scale is defined as the first 20 m above the ground. The forest canopy is a unique photochemical environment due to the attenuation of radiation, generation of smaller scale eddies, and large surface areas for deposition of gases and aerosol [*Gao et al.*, 1993]. The combination of an emission profile near the surface and stagnant conditions caused by forest elements results in large biogenic hydrocarbon mixing ratios in the canopy. In turn, the rates of gas-phase photochemical reactions in the canopy depend non-linearly on gaseous mixing ratios. Regional air quality and climate models use large scale grid cells, typically on the order of tens of kilometers by tens of kilometers, resulting in emissions being instantaneously diluted into large volumes with photochemistry occurring on ensemble grid-cell averages [*Makar et al.*, 2003]. Biogenic emission processing systems have incorporated the escape efficiency into the calculation of grid volume emission to account for canopy scale photochemical loss [*Pierce et al.*, 1998; *Guenther et al.*, 1999]. *Makar et al.* [1999] used a one-dimensional canopy model to calculate an isoprene escape efficiency of 0.60 for a mixed deciduous forest in southern Ontario illustrating that significant chemical loss of isoprene may occur on the canopy-scale. Near-field sources of biogenic hydrocarbons due to weak diffusive transport were shown to impact isoprene mixing ratios at the Borden site in southern Ontario. Conversely, *Doskey and Gao* [1999] used a coupled diffusion-chemistry model to calculate canopy-scale isoprene vertical profiles and canopy top fluxes for a deciduous forest which agreed closely with results from a non-reactive simulation. Isoprene chemical oxidation played a more significant role in altering vertical profiles and fluxes in the middle and upper boundary layer. In summary, there is still a great deal to be learned about the identity of reactive biogenic emissions and their interactions with radicals, oxidants and aerosol.

[5] The goal of the present study was two-fold. First, we used a one-dimensional canopy model to calculate escape efficiencies for terpenoid emissions from a Loblolly Pine plantation in North Carolina for conditions during the CELTIC field study. The CELTIC field program was designed to look at the **C**hemical **E**mission, **L**oss, **T**ransformation and **I**nteraction within **C**anopies. This paper is motivated by a need for 1) an improved understanding on how canopy-scale photochemistry impacts biosphere-atmosphere exchange and, 2) the development of escape efficiency parameterizations for regional air quality and climate models. The second goal of this paper was to characterize the photochemical environment in the forest canopy by calculating vertical profiles for radical production rates and ozone production and loss rates. A representative sesquiterpene emission, β-caryophyllene, was added to the canopy model to represent the missing reactive terpene emission recently inferred by *Di Carlo et al.* [2004] and *Holzinger et al.* [2004]. The impact of terpene ozonolysis on radical production and ozone loss will be discussed.

2. Methodology

2.1. Site Description

[6] CELTIC took place at the Duke Forest C-H2O Research Site in North Carolina (35.98°N, 79.09°W). Duke Forest is a Loblolly Pine plantation (*Pinus taeda*) with approximate tree heights of 18 m and tree spacing of 2.0 m × 2.4 m. The site consists of six free-air CO_2 enrichment (FACE) rings, three of which provide elevated atmospheric CO_2 concentrations, and three represent ambient control rings. Trace gas measurements were performed at control ring 6 on a 26 m tower. The plantation is approximately 330 m × 800 m in dimension with ring 6 having a fetch of ~500 m for predominant wind directions from the southwest. Detailed footprint analysis [*Karl et al.*, 2004] suggests that in-canopy air masses were influenced significantly by local emissions from within the plantation. Duke Forest is located between the towns of Chapel Hill (10 km to the southeast), Durham (20 km to the northeast), Raleigh (40 km to the southeast) and Burlington (30 km to the northwest). The closest major highway is I-40 (2.4 km to the northeast).

2.2. Measurement Intensive Period

[7] This analysis interprets observations from an intensive period on 24 July 2003 where proton-transfer reaction

Table 1. List of Measurements Used to Constrain and Validate the Canopy Model Along With Typical Midday Conditions for 24 July 2003

Measurement	Technique	Model Constraint or Validation	Typical Midday Range (Canopy Top to Bottom)	Principle Investigator
Water Vapor	Dew Point Hygrometer	Vertically Constant, Updated Δt = 30 min	1.9×10^7 ppbv	Guenther
NO_x	Chemi-luminescence	Vertically Distributed, Updated Δt = 30 min	1.8–1.6 ppbv	Fuentes Toohey
O_3	Chemi-luminescence	Vertically Distributed, Updated Δt = 30 min	50–42 ppbv	Fuentes Toohey
Ethane	GC-MS	Vertically Constant. Updated Δt = 30 min	1.0 ppbv	Fuentes
Propane	GC-MS	Vertically Constant. Updated Δt = 30 min	0.4 ppbv	Fuentes
C_4-C_5 Alkanes	GC-MS	Vertically Constant. Updated Δt = 30 min	0.3 ppbv	Fuentes
C_6-C_8 Alkanes	GC-MS	Vertically Constant. Updated Δt = 30 min	0.03 ppbv	Fuentes
Ethene	GC-MS	Vertically Constant. Updated Δt = 30 min	0.2 ppbv	Fuentes
Terminal Alkenes	GC-MS	Vertically Constant. Updated Δt = 30 min	0.1 ppbv	Fuentes
Internal Alkenes	GC-MS	Vertically Constant. Updated Δt = 30 min	0.03 ppbv	Fuentes
Toluene	PTR-MS, GC-MS	Vertically Constant. Updated Δt = 30 min	0.05 ppbv	Fuentes
Di-substituted Aromatics	PTR-MS, GC-MS	Vertically Constant. Updated Δt = 30 min	0.02 ppbv	Fuentes
Tri-substituted Aromatics	PTR-MS, GC-MS	Vertically Constant. Updated Δt = 30 min	0.02 ppbv	Fuentes
VOC Profiles: Isoprene, Pinene, MACR+MVK	PTR-MS, Inlet on Pulley	Validation	ISOP 1.5–2.1 ppbv PINENE 0.3–0.8 ppbv MACR + MVK 2.0–1.7 ppbv	Karl
Canopy Top HCHO	PTR-MS	Validation	2.0–2.3 ppbv midday	Karl
Canopy Top Fluxes: Isoprene Pinene	Eddy Covariance with PTR-MS	Validation	ISOP 0.62 mg/m^2/hr PINENE 0.68 mg/m^2/hr	Baker Karl
Isoprene Basal Rates	Leaf-level Cuvette, GC-FID	Calculated Vertically as a function of LAI	100–60 μg/g/hr for Sweet Gum	Potasanak
Pinene Basal Rates	Leaf-level Cuvette, GC-FID	Constant Model Input	3 μg/g/hr Loblolly Pine 3 μg/g/hr Sweet Gum	Geron
Leaf Area	Ground Litter and Optical	Vertically Distributed	Sweet Gum 1.2 m^2/m^2 Loblolly Pine 2.7 m^2/m^2	Oren
PAR	LI-COR	Vertically Distributed Updated Δt = 30 min	2000–100 μmol/m^2/s	Stroud
J-Values	J(NO_2) Radiometer UV-B Biometer	Vertically Distributed Updated Δt = 30 min	J(NO2) 7.0×10^{-3} – 3.5×10^{-4} s^{-1} J(O1D) 3.4×10^{-5} – 1.7×10^{-6} s^{-1}	Stroud
O_3 Column	TOMS	Updated Daily	310 DU	NASA
Aerosol Optical Depth	Shadow Band UV Radiometer	Updated Daily	τ(368 nm) = 0.5	USDA CSU
Friction Velocity	Sonic Anemometer	Vertically Distributed Updated Δt = 30 min	0.4–0.05 m/s	Nemitz Turnipseed
Vertical Velocity Variance	Sonic Anemometer	Vertically Distributed Updated Δt = 30 min	0.5–0.05 m/s	Nemitz Turnipseed

mass spectrometry (PTR-MS) vertical profile measurements were available [*Karl et al.*, 2004]. Midday conditions during the measurement intensive (10:00–14:00 EST) were partly sunny with temperature and relative humidity in the range 22.4–26.8°C and 53–73 %, respectively. The 30-minute averaged canopy-top PAR also ranged from 1321–2104 μmol/m^2/s.

2.3. Measurement Description

[8] Table 1 summarizes the measurements used to constrain and validate the canopy model. A range from the top of the canopy to the bottom is shown for typical midday conditions on 24 July 2003 where the analytical techniques provide data vertically within the canopy. Otherwise, typical values are presented for the canopy top. The references listed contain further details on the measurement techniques.

2.4. Canopy Modeling

[9] The canopy model was one–dimensional with a domain of 1001 m and 1 m vertical resolution. Second order accurate operator splitting was used to solve the following system of equations

$$\frac{\partial C_{i,j}}{\partial t} = E_{i,j} + f_{i,j} + \frac{\partial}{\partial z}\left(\kappa(z_i)\frac{\partial C_{i,j}}{\partial z}\right) \quad (1)$$

where $C_{i,j}$ is the concentration of the ith chemical species in the jth model layer, $\kappa(z_j)$ is the eddy diffusivity, $f_{i,j}$ is the ith

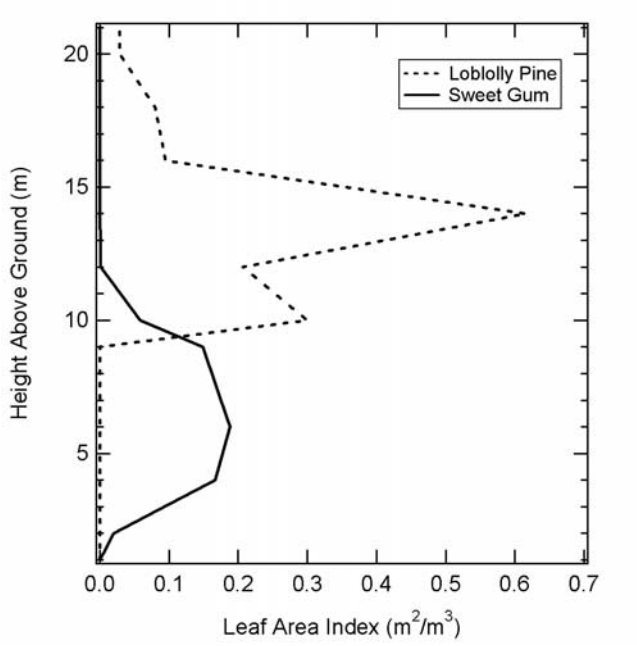

Figure 1. Leaf area profile for the over story of Loblolly Pine and the under story of Sweet Gum at Duke Forest, North Carolina.

species' rate of change due to chemical reactions in the *j*th layer, and $E_{i,j}$ is the *i*th species' rate of change due to emissions into the *j*th model layer. Radiative transfer calculations also impact both the $E_{i,j}$ and $f_{i,j}$ operators. Each portion of (1) is operator split. Chemical reactions and emissions were included within the same operator ($A_{C,E}$) with diffusion making up the remaining operator (A_D). The order of a time step (Δt = 1 min) was

$$A_D\left(A_{C,E}\left(A_{C,E}(A_D(C))\right)\right) \quad (2)$$

where the diffusion operator was divided into two sub–steps (each 30 s) performed at the beginning and end of the time step. Environmental conditions used to constrain the canopy model where updated every 30 min. Further details of the canopy model can be found in *Makar et al.* [1999]. Improvements to the canopy model for this study are described below.

2.5. Canopy Leaf Area Profile and Basal Emission Rates

[10] Leaf-level emissions were simulated using the algorithms of *Guenther et al.* [1993] and *Guenther* [1997]. These emission algorithms include a dependence on the leaf area index, leaf density, basal emission rate, temperature and PAR. The basal emission rate is defined at a temperature of 303.15 K and for a PAR value of 1000 μmol m^{-2} s^{-1}. Figure 1 illustrates the leaf area profiles by species type at Duke Forest measured by light extinction, destructive harvesting and leaf litter. The over story is dominated by Loblolly Pine (dashed trace) with significant leaf area between heights of 8–17 m. The under story is predominately native Sweet Gum (*Liquidambar styraciflua*, solid trace) with significant leaf area between heights of 2–11 m. Leaf-level basal emission rates were measured on-site for both species. For the Loblolly Pine, a basal emission rate of 3 μg/g/hr was used for α,β-pinene. The two isomers of pinene were treated as a surrogate species due to the inability of the PTR-MS measurement technique to distinguish isomers. This introduces some uncertainty in our analysis because the different isomers of pinene react with oxidants at different rates and thus will not have identical escape efficiencies. Here, we assume that α,β-pinene react as if the surrogate were the most abundant isomer in the atmosphere, α-pinene. β-Caryophyllene was chosen as a representative species for sesquiterpene emission and was assigned a basal emission rate of 1 μg/g/hr (recommended by P. Harley based on unpublished laboratory cuvette measurements not specific to Duke Forest, personal communication). A sensitivity simulation with a β-caryophyllene basal emission rate of 30 μg/g/hr was also performed to represent conditions inferred by *Holzinger et al.* [2004] where sesquiterpene emissions are an order of magnitude larger than monoterpene emissions. Loblolly Pine leaf densities were measured at 230 g/m^2. For Sweet Gum, isoprene basal emission rate measurements during CELTIC suggested a basal rate dependence on canopy height. As a result, an isoprene basal emission rate expression as a function of canopy shading (expressed in turn as a function of cumulative leaf area index with height) was generated based on leaf-level cuvette emission measurements performed at different canopy heights at Duke forest (y = 68/60(151 − 19×) where the 68/60 factor converts carbon mass to isoprene mass, x is the dimensionless cumulative leaf area index, and y is the isoprene basal emission with units of μg/g/hr; correlation coefficient R = −0.48). The negative slope reflects the observation that basal emission rate increased towards the top of the canopy, since the prior history of leaf-level exposure to radiation impacts instantaneous basal emission rates. The measured leaf area index profile was used along with the above expression to calculate isoprene basal emission rates for each model height level. In the model, α,β-pinene was also emitted from Sweet Gum with a basal emission rate of 3 μg/g/hr. Sweet Gum leaf densities were measured at 50 g/m^2. Leaf temperature at each model layer was assumed equal to measured air temperature and interpolated to the model grid from four measurement heights.

2.6. Canopy Radiative Transfer

[11] Measurements of $J(NO_2)$, UV-B and PAR were made at the top of the canopy and simultaneously at various heights within the canopy throughout the field program. The $J(NO_2)$ signal was measured with filter radiometers (Metcon Inc.). The UV-B signal was measured with UV-Biometers (Model 501, Solar Light Co.). PAR was measured with LICOR quantum sensors (model LI-190SA, LiCor Inc.). The $J(NO_2)$ and UV-B sensors were calibrated immediately after the field program against a spectrophotometer [*Shetter et al.*, 2003]. Excellent correlations were observed between the radiometer $J(NO_2)$ signal and the spectrophotometer $J(NO_2)$ and between the radiometer UV-B signal and the spectrophotometer $J(O^1D)$; thus, the spectrophotometer J-values were used to calibrate the radiometer signals. Manufacturer calibrations were used for the PAR sensors. Figure 2 presents the canopy extinction measurements (ratio of in-canopy to canopy top measurement) for $J(NO_2)$

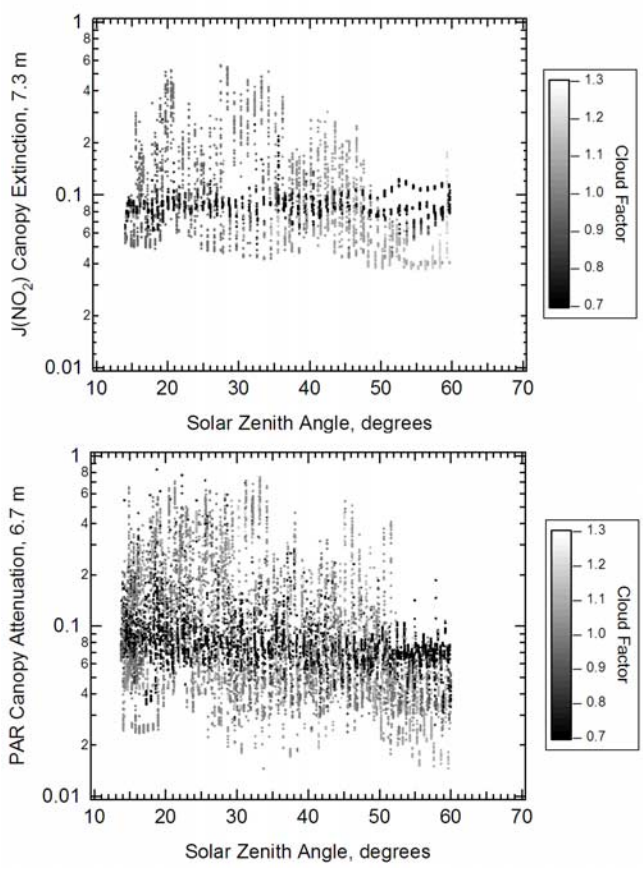

Figure 2. Measured attenuation of radiation (defined as the observed irradiance within the canopy divided by observed irradiance at canopy top) as a function of solar zenith angle. (a) For $J(NO_2)$ at 7.3 m. (b) For PAR at 6.7 m. Data are color-coded as a function of a cloud factor (defined as the observed canopy top irradiance divided by clear-sky irradiance).

(Figure 2a) and PAR (Figure 2b). The data are also color-coded as a function of a cloud factor (CF) defined as the ratio of the canopy top observed irradiance to the clear-sky canopy top irradiance. Here a reconstruction of the clear-sky canopy top J-values was derived from a 1-D atmospheric radiative transfer model (TUV [*Madronich et al.*, 1998]) with modeled aerosol properties optimized to recreate observations for periods of clear-sky measurements. For cloudy periods, the TUV modeled clear sky values were used to estimate the denominator in the cloud factor calculation. O_3 column densities for daily input into TUV were derived from the TOMS database (http://toms.gsfc.nasa.gov/). A surface albedo of 0.1 was assumed for the Loblolly Pine plantation. Considering all the data in Figure 2, a gradual decreasing trend was observed in canopy extinction ratio with increasing solar zenith angle. The considerable scatter is due to the non-homogeneity in canopy foliage. However, the color coding suggests there is a further dependence to the trend and scatter as the measurement points recorded under cloudy conditions (red points) show considerably less scatter and little dependence of solar zenith angle. This is indicative of the isotropic nature of diffuse radiation in the canopy. For clear sky conditions (green points), the canopy radiation has both direct and diffuse components. The direct component has a cosine dependence on solar zenith angle. The high degree of variability in the direct component (green points, $0.9 < CF < 1.1$) is due to the non-homogeneity of the canopy structure relative to direct beam. Within the canopy model, the canopy top J-values for all the chemical species were derived from the 1-D radiative transfer model with applied cloud correction factors. Measured canopy top PAR values were directly implemented into the canopy model. The attenuation of radiation at each height level within the canopy was modeled by multiplying the canopy top values by the canopy extinction factor:

$$Extinction\ Ratio(z) = Direct\ Fraction \exp\left(\frac{\tau_{VERT}(z)}{\cos\theta}\right) + Diffuse\ Fraction \exp(\tau_{DIF}(z)) \quad (3)$$

where the canopy top diffuse and direct fractions of the radiation were derived from TUV and parameterized into the canopy model as a function of the cloud factor. The vertical and diffuse optical depths were derived from fits to the data in Figure 2 for data separated into clear and cloudy sky periods. Table 2 lists the vertical and diffuse optical depths for $J(NO_2)$, $J(O^1D)$ and PAR for different heights and leaf area indices in the canopy. A linear correlation of vertical and diffuse optical depths as a function of leaf area index was parameterized into the canopy model to calculate canopy extinction ratios at each height level.

[12] The observed PAR and J-values were sorted based on solar zenith angle for each height to perform model-measurement evaluations. Figure 3 illustrates the vertical profiles of canopy extinction ratio at solar zenith angles of 16 ± 4 (green points) and 56 ± 4 (red points). The canopy model profiles were calculated for both clear-sky conditions (using the above canopy TUV diffuse and direct fractions, solid lines) and cloudy conditions (direct fraction is negligible, dashed lines) to illustrate the possible variability due to cloud cover conditions. Only modeled profiles for PAR are included in Figure 3 to simplify the plot. Modeled lines for the J-values and PAR were very similar due to the small differences in optical depths for PAR and the J-values.

[13] While the radiation sensors stay fixed on a horizontal plane, the leaf surfaces are more randomly distributed relative to the solar beam. In the canopy model, we used a spherical leaf angle distribution which assumes that the average leaf angle between perpendicular to the leaf surface and direct solar beam is 60° and that each leaf intercepts

Table 2. Vertical and Diffuse Optical Depths Calculated From the Measurements of $J(NO_2)$, J(O1D), and PAR at Different Height Levels in the Canopy

Height, m	Vertical τ PAR	Vertical τ $J(NO_2)$	Vertical τ J(O1D)	Diffuse τ PAR	Diffuse τ $J(NO_2)$	Diffuse τ J(O1D)
14.6				0.47	0.37	
12.8				0.59		0.40
10.9				1.7	1.4	
7.3				2.4	2.4	
6.7	1.7		1.6	2.7		2.4
2.7	2.8		2.7	3.6		3.1
1.8	2.1	3.1		2.9	2.9	

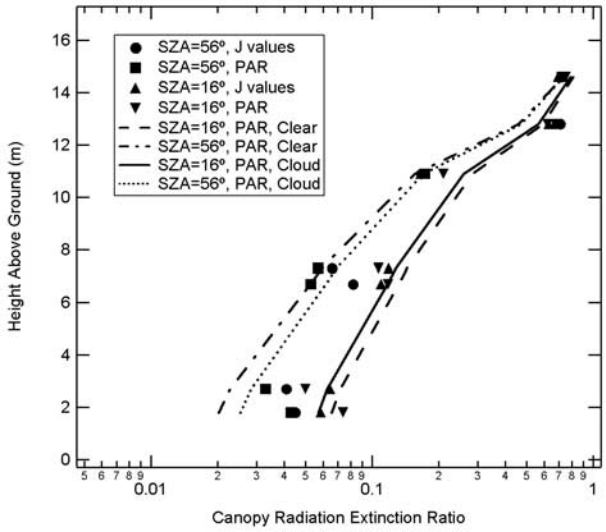

Figure 3. Model and measurement comparison for the vertical profile of canopy attenuation. Symbols represent measured J-values for two different solar zenith angles (red points are 56°, and green points are 16°). Red and green lines are modeled results for the two different solar zenith angles with the spread between the dashed and solid lines representing the transition from cloudy to clear sky conditions.

half of the direct incoming solar beam [*Guenther et al.*, 1999]

2.7. Vertical Diffusive Transport

[14] The atmospheric transport within the canopy model was based on a modified K-theory of vertical turbulent diffusion [*Raupach*, 1989]:

$$\frac{\partial C}{\partial t} = -\frac{\partial}{\partial z}\left(R(\tau)\sigma_w^2 T_L \frac{\partial C}{\partial z}\right) \quad (4)$$

where the eddy diffusivity ($K = \sigma_w^2 T_L$) is modified by the factor R, which accounts for canopy effects on turbulence (so-called ''near-field'' effects). The variable R is dependent on the magnitude of the Lagrangian timescale defined as $T_L = 0.3hc/u^*$ [*Raupach*, 1988] and the ratio of τ/T_L, where τ is a transport lifetime [*Makar et al.*, 1999]:

$$R = \frac{[1 - \exp(-\tau/T_L)](\tau - T_L)^{3/2}}{[\tau - T_L + T_L \exp(-\tau/T_L)]^{3/2}} \quad (5)$$

Above the canopy to the top of the boundary layer, K-values from *Gao et al.* [1993] were used to obtain the eddy diffusivities, as in *Makar et al.* [1999]. Figure 4a presents the observations for the vertical velocity standard deviation (σ_W) for 4 different heights as measured with sonic anemometers (ATI, RM Young). Linear interpolations for σ_W were used to constrain each modeled grid level. A τ/T_L value of 1.17 in the canopy, as used in *Makar et al.* [1999], was found to result in a significant modeled overestimate of peak isoprene and α,β-pinene within the canopy. Here, a τ/T_L of 4 was found to optimize the model-measurement comparison for both isoprene and α,β-pinene, which results in an R factor near unity. This difference could be due to differences in the canopy structure or the fumigation system operated at the Duke Forest. The Crank-Nicholson numerical scheme was used for solving the diffusion equation (4). This scheme enabled either a constant surface flux or deposition velocity to be prescribed as boundary conditions. The O_3, HNO_3, and NO_2 dry deposition velocities were taken as 0.4, 4, and 0.1 cm/s [*Jacobson*, 1999]. Deposition velocities for VOCs were optimized based on measured mixing ratio vertical profiles near the surface (see section 3.1).

2.8. Canopy Photochemistry

[15] The canopy model gas-phase chemical mechanism for isoprene and α,β-pinene are described in *Makar et al.* [1999]. A simplified treatment for β-caryophyllene loss was introduced into the canopy model based on available laboratory data as summarized in *Atkinson and Arey* [2003]:

(R1) $\beta\text{-CARY} + O_3 \rightarrow 0.14\text{HCHO} + 0.06\text{OH} + 0.16\text{MUCN}$
$k = 2.1 \times 10^{-14}\text{cm}^3/\text{molec/s}$

where MUCN represents unsaturated dicarbonyl species. The remaining products have not been quantified in the laboratory and are assumed to partition entirely to the aerosol phase (not included in gas-phase mechanism). As a sensitivity test, an NO_3-initiated β-caryophyllene loss reaction with a rate coefficient of 2.2×10^{-11} cm^3/molec/s was also added to the mechanism (see section 3.4). Heterogeneous chemistry as outlined in *Jacob* [2000] was also implemented into the gas-phase mechanism where aerosol surface area concentrations where derived from scanning mobility particle sizer measurements during CELTIC:

(R2) $N_2O_5 + \text{aerosol} \rightarrow 2\ HNO_3 \quad \gamma = 0.1$

(R3) $NO_3 + \text{aerosol} \rightarrow HNO_3 \quad \gamma = 10^{-3}$

(R4) $HO_2 + \text{aerosol} \rightarrow 0.5\ H_2O_2 \quad \gamma = 0.2$

(R5) $NO_2 + \text{aerosol} \rightarrow 0.5\ \text{HONO} + 0.5\ HNO_3 \quad \gamma = 10^{-4}$

3. Results and Discussion

3.1. Biogenic Hydrocarbon Vertical Profiles

[16] Figure 5 illustrates the comparison between the modeled and observed isoprene mixing ratio profiles for daytime conditions on 24 July 2003. Solid and dashed lines represent observed and modeled data, respectively. The temporal trend in the observed profiles was captured quite well in the modeled results. For example, the 10:00–10:30 EST observed and modeled profiles were both local minimum (yellow solid line) while the 13:00–13:30 EST observed and modeled profiles were both local maximum (green solid line). The observed vertical distribution of isoprene mixing ratio was also captured by the model with similar magnitude peak mixing ratios between 3 and 6 m.

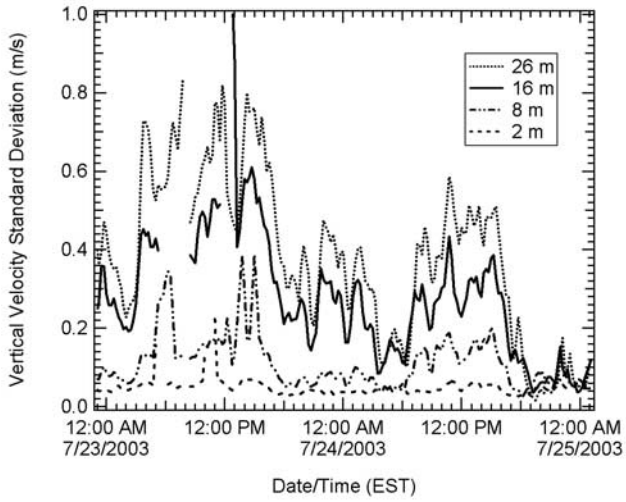

Figure 4. Observed time series for vertical velocity variance and friction velocity for four different canopy heights (2, 8, 16, and 26 m).

An interesting trend was observed near the surface with isoprene mixing ratios generally decreasing from a height of ~3–5 m, down to the surface. Preliminary model simulations with no surface fluxes resulted in peak maximum isoprene mixing ratios at the surface. It was necessary to incorporate a surface deposition flux in the model with an isoprene deposition velocity of 0.2 cm/s to simulate the observed isoprene trend near the surface. This deposition velocity is substantially smaller than values adopted by *Jacob and Wofsy* [1988], however, significantly higher than assumed by traditional deposition models [e.g., *Wesely*, 1989]. *Cleveland and Yavitt* [1997] observed that soil microbes can consume isoprene and calculated deposition velocities which are in the same range as values adopted in the current study. Current regional air quality models generally do not include an isoprene deposition flux. At the site, the deposition flux was a negligibly small fraction of the canopy top isoprene flux; however, on a regional scale incorporating an isoprene deposition flux of this magnitude may have a significant impact on the dispersion of isoprene from forested environments.

[17] Figure 6 shows the comparison between the modeled and observed α,β-pinene vertical profiles for daytime conditions during the measurement intensive. An approximate linear decrease in α,β-pinene mixing ratio was observed between the top of the canopy and 3 m above the ground. This vertical distribution was also observed in the modeled results. Interestingly, between 3 m and the ground, α,β-pinene mixing ratios increased more sharply. Physically, this likely represented an emission of α,β-pinene from pine needles scattered on the ground. A modeled surface flux of 8.5×10^9 molec/cm^2/s was used to represent this increase in observed surface α,β-pinene mixing ratio. This surface flux represented 10% of the canopy top flux for α,β-pinene.

3.2. Model Validation: Oxidation Product Vertical Profiles

[18] Figure 7 shows a comparison between the modeled and observed vertical profiles for the sum of the methacrolein (MACR) and methyl vinyl ketone (MVK) mixing ratio for the measurement intensive period. MACR and MVK are isomers resulting in the PTR-MS technique measuring the sum of their concentrations. The PTR-MS sensitivity to each isomer is within 15%. Thus, no concentration ratio was assumed in measuring the sum of their concentrations from measured ion signals. The modeled results were similar to

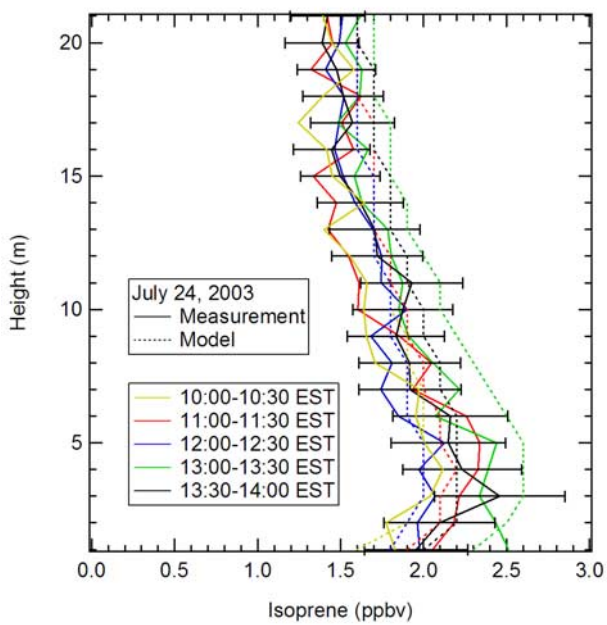

Figure 5. Comparison of modeled and observed isoprene vertical profiles for daytime conditions during the (a) 17 July 2003 and (b) 24 July 2003 measurement intensive periods.

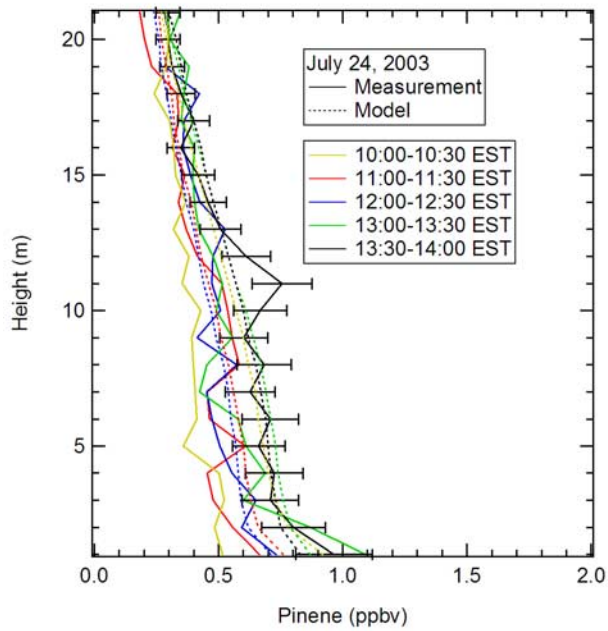

Figure 6. Comparison of modeled and observed α,β-pinene vertical profile for daytime conditions on 24 July 2003.

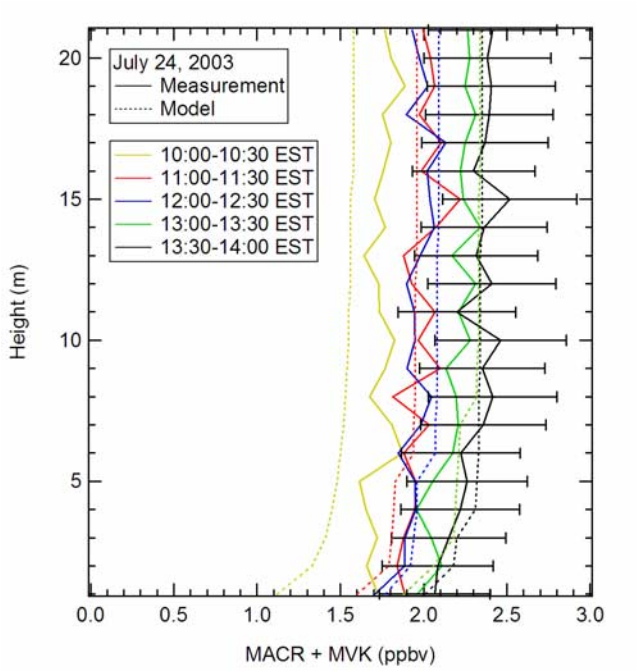

Figure 7. Comparison of modeled and observed vertical profile for the sum of the methacrolein and methyl vinyl ketone mixing ratio during the daytime 24 July 2003 measurement intensive period.

the observations with the model capturing the temporal increase in the isoprene oxidation products between 10:00 and 13:30 EST. A model deposition velocity of 0.2 cm/s was necessary to simulate the observed decrease in mixing ratio near the surface. This is close to values reported by *Karl et al.* [2004], who used a combination of eddy covariance and in-canopy gradient measurements, to infer deposition velocities of 0.45 ± 0.15 cm/s for MVK+MACR above a tropical ecosystem. Recently, *Rottenberger et al.* [2004] suggested similar magnitude deposition velocities for other short-chain aldehydes, namely formaldehyde and acetaldehyde. The general agreement between the modeled results and observations for these isoprene oxidation products suggests the model is reasonably capturing the initial stages of isoprene photochemical conversion within the canopy.

3.3. Role of Photochemistry in Modifying Vertical Profiles and Canopy Top Fluxes

[19] Simulations were performed with no chemistry operator to assess the impact that photochemistry has on vertical profiles and canopy top fluxes. Figure 8 shows modeled vertical profiles for isoprene (Figure 8a), α,β-pinene (Figure 8b), and β-caryophyllene (Figure 8c) with the chemistry operator activated (solid line) and not activated (dashed line). For our base case, only small differences in mixing ratio (less than 10%) were observed for the isoprene and α,β-pinene vertical profiles. Much more significant differences were observed for the β-caryophyllene mixing ratio. Figure 9 illustrates the cumulative impact of the canopy photochemistry on model-derived escape efficiencies. In Figure 9, the base case is labeled as the regional case given that Duke Forest is a moderately polluted site impacted by pollution transported from regional scale sources. Canopy escape efficiencies were calculated at 0.90 and 0.93 for isoprene and α,β-pinene, respectively, suggesting that the transport time scale is considerably faster than the chemical loss timescale for these species. However, for β-caryophyllene, a canopy escape efficiency of 0.30 was calculated. This value suggests a rapid conversion of β-caryophyllene to its oxidation products on the timescale of vertical diffusive transport out of the canopy. The modeled estimate is remarkably similar to the measured values reported by *Ciccioli et al.* [1999] for β-caryophyllene escape from orange orchards in the Valencia citrus belt. They observed a difference between measured canopy top fluxes and leaf-level emissions of a factor of three. Inter-

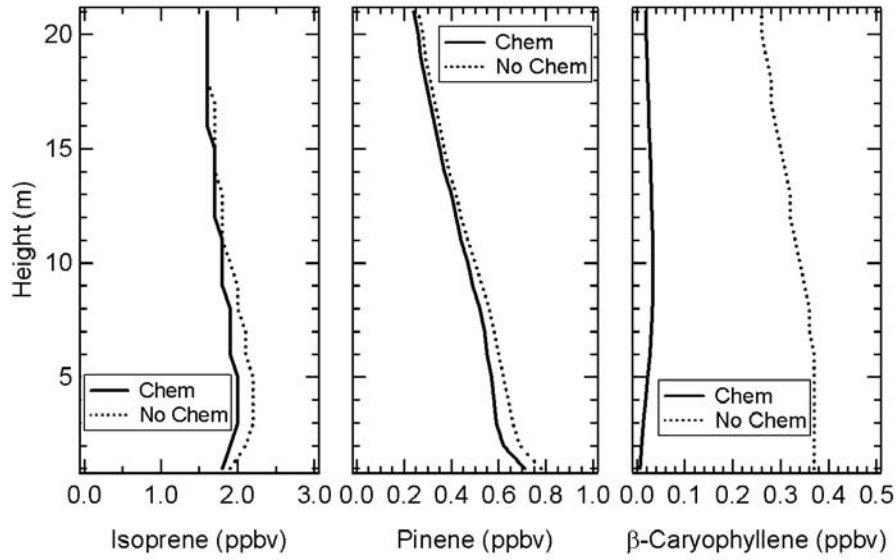

Figure 8. Simulation of the 12:30–13:00 EST period on 24 July 2003 with and without the chemistry operator included in the canopy model.

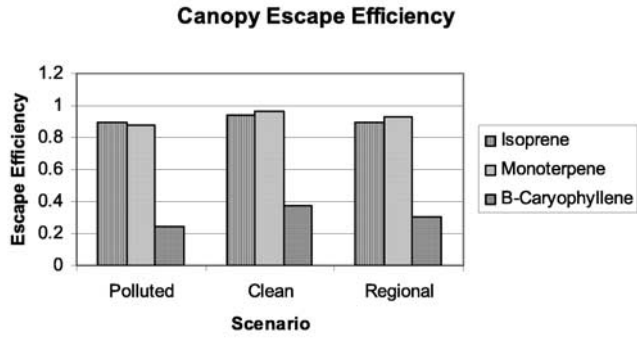

Figure 9. Modeled canopy escape efficiencies for isoprene, pinene and β-caryophyllene for base case (regional) and other pollution scenarios (clean and polluted).

estingly, they did not observe β-caryophyllene oxidation products at canopy top suggesting its products were quickly lost to surfaces (aerosol, non-stomata and ground) in the canopy or further reacted to higher order products. E. Nemitz et al. (2005) measured canopy top aerosol fluxes during CELTIC and observed a complex bidirectional behavior. Particle fluxes measured with an aerosol mass spectrometer at selected mass to charge ratios, consistent with terpene oxidation products, showed upward fluxes for midday conditions. Collectively, results suggest it is important to include escape efficiency estimates for sesquiterpenes within biogenic emission processing systems for regional air quality models.

3.4. Biogenic Hydrocarbon Photochemical Loss Pathways

[20] The relative importance of the various chemical loss pathways for biogenic VOCs varies considerably within the canopy, compared to above the canopy due to the canopy attenuation of radiation. Figure 10 illustrates the model-derived vertical profiles for isoprene (Figure 10a), α,β-pinene (Figure 10b), and β-caryophyllene (Figure 10c) loss by OH, O_3, and NO_3-initiatied oxidation for midday conditions during the measurement intensive period. Isoprene loss at the top of the canopy is dominated by OH-kinetics; however, the combination of an order of magnitude decrease in OH at the surface, a generally uniform O_3 profile and an increasing NO_3 profile toward the surface resulted in similar magnitude OH, O_3, and NO_3-initiated isoprene loss rates near the surface. α,β-pinene loss rates showed a highly structured behavior with OH- and O_3-kinetics dominating near the top of the canopy and O_3- and NO_3-kinetics controlling near the surface. Finally, β-caryophyllene loss is dominated by O_3-kinetics for all heights in the canopy with a peak loss rate observed near the β-caryophyllene maximum mixing ratio at 14 m.

3.5. Canopy Radical Production Rates

[21] Modeled vertical profiles for the important net radical production rates are shown in Figure 11 for midday conditions during the measurement intensive period. At the top of the canopy, the O_3 photolysis channel ($O^1D + H_2O \rightarrow 2OH$) dominated net radical production (17 pptv/min) with formaldehyde photolysis, α,β-pinene ozonolysis and β-caryophyllene ozonolysis of minor importance all in the range 1–3 pptv/min. Interestingly, near the surface, α,β-pinene ozonolysis controlled radical production (3 pptv/min) with the O_3 photolysis channel of secondary importance (1.3 pptv/min). Near the β-caryophyllene mixing ratio peak at 10 m, its contribution to radical production increased to 3 pptv/min about 30% of the O_3 photolysis contribution. Numerous studies have suggested that the ozonolysis of terpenes is the dominant source of radical production in the canopy at night [*Bey et al.*, 2001; *Sillman et al.*, 2002; *Kanaya et al.*, 2002; *Di Carlo et al.*, 2004; *Holzinger et al.*, 2004]. Here, modeling results indicate that even during daytime conditions the terpenoid ozonolysis contribution to canopy scale radical production is significant (35%) for an accumulated canopy calculation.

3.6. Canopy Odd Oxygen Production Rates

[22] Figure 12a presents the modeled vertical profiles for O_3, NO and NO_2 for midday conditions during the mea-

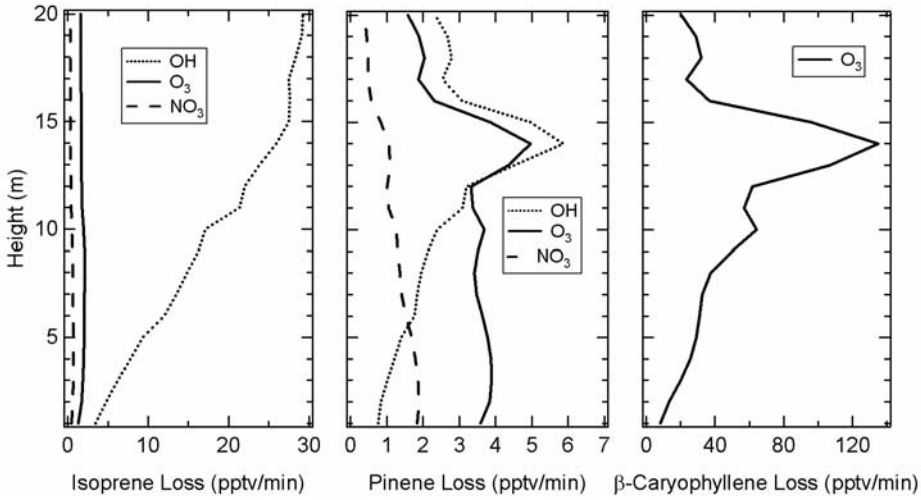

Figure 10. Vertical profiles of OH, O_3, and NO_3-initiated photochemical loss pathways for isoprene, α,β-pinene, and β-caryophyllene during the 12:30–13:00 EST period on 24 July 2003.

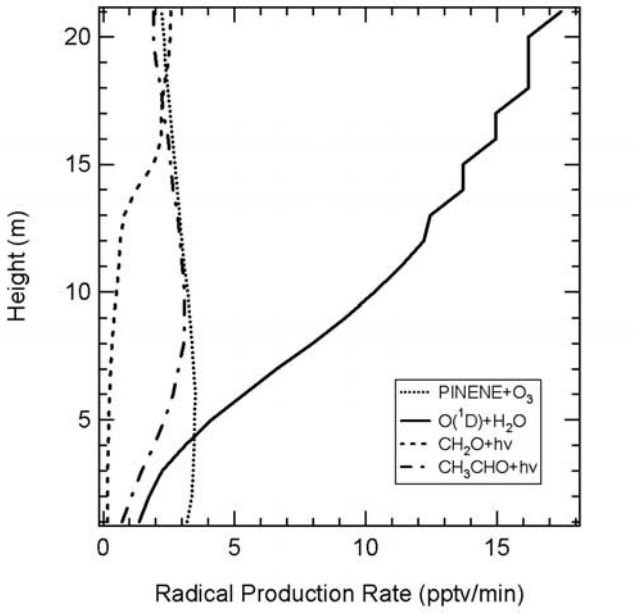

Figure 11. Vertical profiles of modeled radical production during the12:30–13:00 EST period on 24 July 2003.

surement intensive period. Modeled O_3 mixing ratios were 13 ppbv lower at the surface compared to canopy top. We have included the average measured vertical profiles for O_3 and NO_x for the period 13–22 July. Standard deviations are included to represent atmospheric variability. Unfortunately, there were no measurements of O_3 during the intensive period; however, the modeled vertical profile is consistent with the measured O_3 vertical profiles for days measured during the week before the intensive period. Similarly, there were no NO_x measurements available during the intensive period. Here, we constrained the model with typical midday NO_x mixing ratios for days exhibiting similar meteorological conditions, measured 1–3 weeks earlier in June/July 2003. As shown in Figure 12a, little NO_x vertical dependence was observed in the model. This was consistent with NO_x measurements for other periods in June/July 2003.

[23] Figure 12b presents the modeled vertical profiles for O_x production, O_x loss and net O_x chemical change for midday conditions during the measurement intensive period. In the current study, the convention of defining odd oxygen (O_x) as the sum of O_3, O atom and NO_2 mixing ratios was assumed [*Stroud et al.*, 2004]. Table 3 lists the dominant chemical terms in the O_x budget. Near the top of the canopy, net O_x chemical change reached 2.6×10^7 molec/cm^3/s (3.8 ppbv/hr). O_x production was controlled by the HO_2+NO channel followed by the CH_3O_2 + NO and $ISOPO_2$ + NO channels. O_x destruction was dominated by the β-CARY + O_3 channel compared to the $O(^1D)$ + H_2O reaction pathway by a factor of 3.8. Near the surface (1–2 m), net O_x chemical change reached -4.3×10^6 molec/cm^3/s (−0.63 ppbv/hr). O_x production by HO_2 + NO was still the largest term; however, CH_3O_2 + NO, $ISOPO_2$ + NO and TRO2 + NO were only a factor of 3.3, 2.7 and 4.3 smaller, respectively. Near the surface, O_x destruction was dominated by β-caryophyllene ozonolysis and α,β-pinene ozonolysis.

[24] *Kurpius and Goldstein* [2003] used measurements of canopy top O_3 flux and canopy dry deposition to imply the chemical loss of O_3 within the canopy. Their implied O_3 chemical loss followed similar temperature dependence to terpene emission suggesting terpene ozonolysis may be responsible for the O_3 loss. They hypothesized that reactions of O_3 with terpenoid species can make up 51 % of the total canopy loss during the summertime in a pine forest. They estimated an O_3 flux due to non-stomatal chemical loss in the canopy of 20 ± 16 μmol/m^2/hr (3.3×10^{11} molec/cm^2/s). From Figure 12b, we calculated a net positive O_3 chemical production averaged over the canopy height of 0.062 μmol/m^2/hr (9.9×10^8 molec/cm^2/s). Thus, for our base case, gas-phase O_3 chemistry was not contributing significantly to canopy-scale O_3 loss. It should be noted that this estimate depends critically on our basal sesquiterpene emission rate for the surrogate β-caryophyllene. Recently, *Holzinger et al.* [2004] estimated that a reactive terpenoid emission rate 6–30 times greater that the monoterpene emission rate was necessary for closure with measured oxidation products. Given our estimates for basal emission rates (monoterpene equal to sesquiterpene), the negative O_3 mixing ratio profile near the surface in Figure 12a is driven largely by the O_3 deposition flux from the first model layer to the surface. We also calculated gross O_3 chemical loss averaged over the canopy height of 2.9 μm/m^2/hr (4.6×10^{10} molec/cm^2/s). Assuming the dry deposition flux is giving by $F_{O3} = v_D[O_3]$ = (0.4 cm/s)(50 ppbv) = 5×10^{11} molec/cm^2/s, then this chemical loss term represents 9.2% of the dry deposition flux. Integrated over the entire model domain(1 km), the gross O_3 chemical loss was 1.1×10^{12} molec/cm^2/s; a value that exceeds the dry deposition flux by a factor of 2.2.

[25] A sensitivity study was performed with a β-caryophyllene basal emission rate of 30 μg/g/hr representing reactive terpene emissions inferred by *Kurpius and Goldstein* [2003] (order of magnitude larger than our monoterpene emission rate). Integrated over the canopy height, we calculated an average net O_3 chemical loss (largely due to β-caryophyllene ozonolysis and similar to calculated gross O_3 chemical loss rates) of 51 μmol/m^2/hr (8.1×10^{11} and 8.6×10^{11} molec/cm^2/s), which is a factor of 1.6 larger than the estimated dry depositional flux and a factor of 2.6 larger than the *Kurpius and Goldstein* [2003] estimate for non-stomatal chemical O_3 loss at Blodgett Forest. Future measurements of canopy top O_3 flux and reactive terpene concentrations would be helpful to compare with these modeled estimates of stomatal and non-stomatal O_3 net chemical loss. Figure 12a includes the modeled O_3 mixing ratio vertical profile for this sensitivity study. Ground level O_3 mixing ratios were 5 ppbv lower than for our base case; a significant difference but not large enough to recommend a sesquiterpene emission especially given the lack of a measured O_3 profile for this intensive period. This modest O_3 decrease reflects the treatment of longer lived species within the canopy model. Anthropogenic hydrocarbons, H_2O, NO and O_3 were updated to measured and/or assumed regional background values over the entire model domain (1 km) after each time step to reflect the advection of longer lived species to the site. This is a critical model requirement given the small fetch at Duke Forest. Thus, the model set up

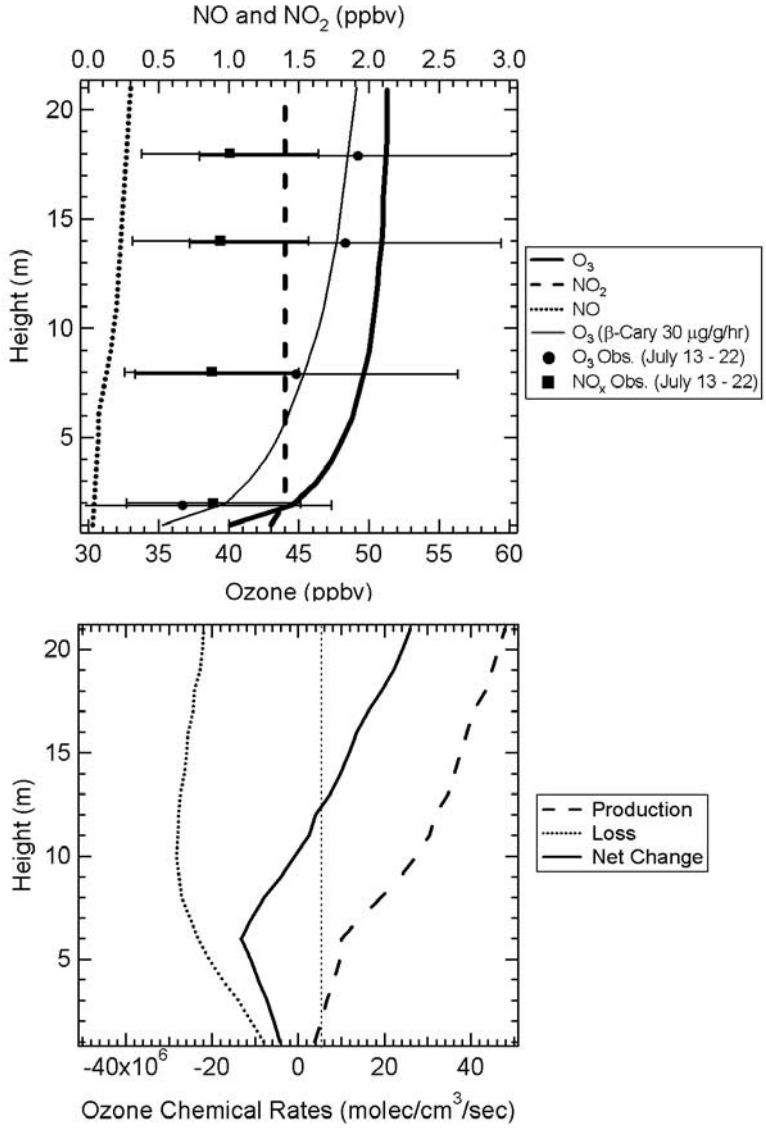

Figure 12. Vertical profiles of modeled O_3, NO_x, O_3 production, O_3 loss, and net O_3 production during the 12:30–13:00 EST period on 24 July 2003. Points represent average mixing ratios and standard deviation limits from observations of NO_x and O_3 for midday conditions (10:00–14:00 EST) between 13 and 22 July.

limits the ability for O_3 to reach a steady state, which is reasonable given that O_3 likely does not reach a steady state with conditions over the plantation. Several shorter lived species formed from β-caryophyllene had significantly larger mixing ratios for this sensitivity study. For example, OH and HCHO, had mixing ratios at the surface of 1.1×10^6 cm^{-3} and 5.9 ppbv, respectively, compared to our base case mixing ratios of 5.4×10^5 cm^{-3} and 2.4 ppbv. Interestingly, observed noontime HCHO mixing ratios at Duke Forest were 2.0–2.3 ppbv, similar to our base case.

[26] Clearly, the site at Duke Forest is not ideal for model-measurement comparison of longer lived species due to its small fetch. Future measurements at a more horizontally homogeneous site would be beneficial for comparison with longer lived species model output. Specifically, OH in addition to VOC and NO_x concentration measurements as well as canopy top O_3 flux measurements combined with

Table 3. Chemical Reaction Rates in the O_x Budget[a]

Reaction	1 m Above Ground	10 m Above Ground	20 m Above Ground
β-CARY + O_3	4.9×10^6	2.1×10^7	1.2×10^7
TERP + O_3	1.8×10^6	1.7×10^6	1.2×10^6
ISOP + O_3	3.4×10^5	2.9×10^5	1.7×10^5
O(1D) + H_2O	2.5×10^5	2.1×10^6	3.2×10^6
HO_2 + NO	1.7×10^6	1.6×10^7	2.7×10^7
CH_3O_2 + NO	5.2×10^5	3.9×10^6	6.3×10^6
ISO_2[b] + NO	6.4×10^5	3.9×10^6	4.7×10^6
TRO_2[c] + NO	4.0×10^5	2.1×10^6	2.5×10^6

[a]Units are in molec/cm^3/s.
[b]ISO_2 is the peroxy radical formed from OH-initiated isoprene oxidation.
[c]TRO_2 is the peroxy radical formed from OH-initiated α,β-pinene oxidation.

Table 4. Anthropogenic VOCs and NO_x Mixing Ratios Used in the Canopy Model for the Three Urbanization Scenarios[a]

Chemical Species	Clean Continental	Regional Continental	Urban Impacted
NO	0.003–0.03	0.03–0.3	0.13–1.3
C_2H_6	0.5	1.0	3.0
C_3H_8	0.2	0.4	1.0
C4-C5 Alkanes	0.1	0.3	22
C6-C8 Alkanes	0.01	0.03	22
C_2H_4	0.066	0.2	0.74
Terminal Bond Alkenes	0.033	0.1	0.42
Internally Bonded Alkenes	0.0075	0.03	0.21
Toluene	0.01	0.05	1.5
Xylenes	0.005	0.02	0.77
Tri-substituted Aromatics	0.005	0.02	0.77

[a]Units are in ppbv.

our present VOC plus NO_y flux measurements would be helpful in constraining an inverse modeled estimate for sesquiterpene emission more accurately.

3.7. Sensitivity Study: Impact of Anthropogenic Pollution of Biosphere-Atmosphere Exchange

[27] An overarching goal of the on-going CELTIC field program is to develop escape efficiency parameterizations for biogenic species under different environmental conditions. Escape efficiency parameterizations could then be implemented into the emission processing systems of regional air quality and climate models. Escape efficiencies are known to vary depending on vertical mixing parameters associated with mechanical and thermal-induced turbulence (e.g., varying friction velocity and turbulent kinetic energy). It is hypothesized that escape efficiencies also depend on atmospheric chemistry parameters associated with gas-phase concentrations and photo-dissociation rates (e.g., varying NO_x and anthropogenic VOCs). A series of sensitivity studies were performed to address the impact that urbanization has on canopy top biogenic fluxes for downwind impacted forests. Here, we defined three scenarios with identical biogenic emissions but differing anthropogenic VOCs and NO_x: (1) a polluted case representative of conditions in Nashville, TN as defined in *Zaveri et al.* [2003], (2) a clean case representative of conditions far removed from NO_x and anthropogenic VOC emissions, and (3) the base case for Duke Forest which represents regional background conditions in the southeastern United States. Table 4 lists the anthropogenic hydrocarbon and NO_x mixing ratios constrained in the model for each scenario. Figure 13 compares the canopy-integrated chemical loss pathways for isoprene, α,β-pinene, and β-caryophyllene for the three scenarios expressed as a percentage contribution. For isoprene integrated loss over the entire canopy, OH-kinetics dominated removal for all three scenarios. For the polluted case, O_3- and NO_3-oxidation contributed about equally and summed to a 25% contribution compared to the 75% contribution from OH-oxidation. For α,β-pinene, an interesting trend emerged with O_3-kinetics dominating for the clean scenario, OH-kinetics dominating for the base case, and NO_3-kinetics dominating for the polluted case. For β-caryophyllene, O_3-initiated loss was the largest term for all the scenarios with NO_3-oxidation only approaching a few percent of β-caryophyllene ozonolysis for the polluted case.

[28] Figure 9 compares the overall canopy escape efficiencies for the three biogenic species for each pollution scenario. For isoprene, escape efficiencies showed only a small sensitivity to anthropogenic pollution levels with a decrease from 0.94 to 0.90 (4% decrease) in comparing the clean to the polluted scenario. Similarly, for α,β-pinene, canopy escape efficiencies decreased from 0.97 to 0.87 (10% decrease) in comparing the clean to the polluted scenario. β-caryophyllene showed a larger sensitivity to anthropogenic pollution levels by decreasing from 0.38 to 0.25 (34% decrease largely due to increases in O_3 mixing ratio) in comparing the clean to the polluted scenario.

4. Conclusions

[29] In this study, we have used a one-dimensional model to scale up leaf-level VOC emissions to canopy top fluxes for conditions during the CELTIC field program. We

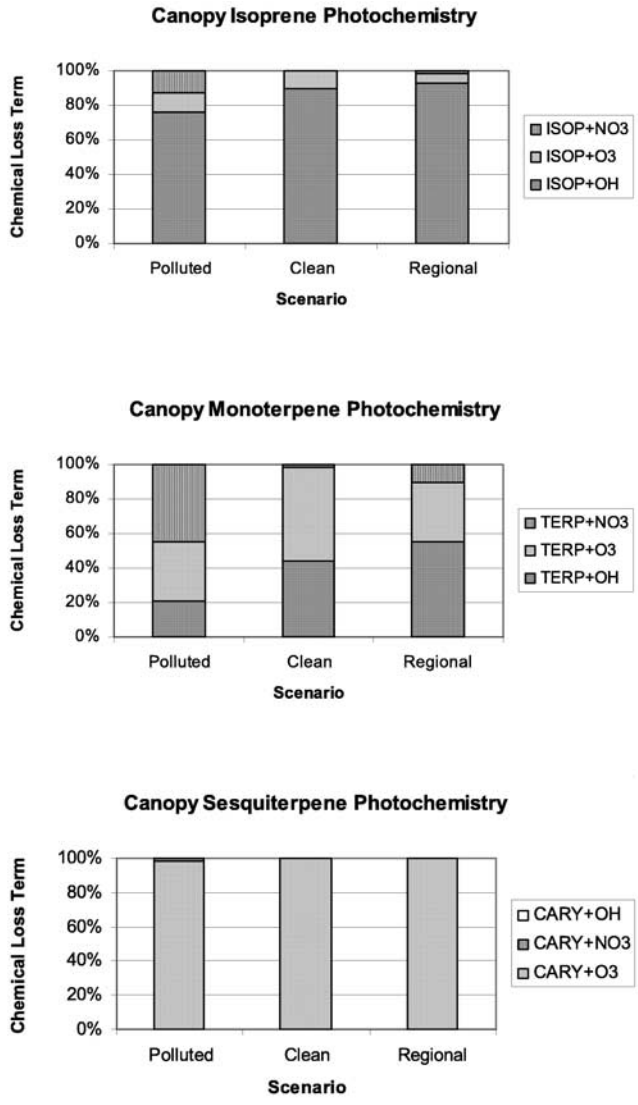

Figure 13. Comparison of canopy-integrated chemical loss pathways for isoprene, pinene, and caryophyllene for three pollution scenarios expressed as a percentage contribution for OH, O_3, and NO_3-initiated pathways.

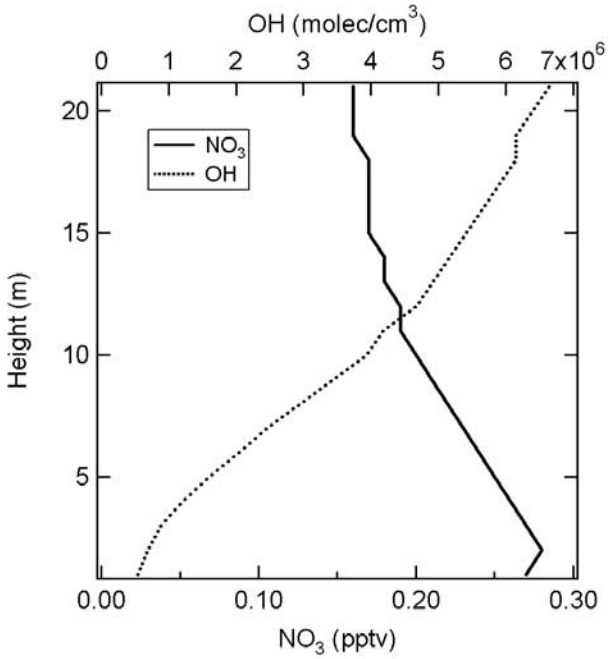

Figure 14. Vertical profiles of modeled NO_3 and OH during the 12:30–13:00 EST period on 24 July 2003.

evaluated the model based on a measurement intensive for midday conditions on 24 July 2003 at Duke Forest. After the canopy model was validated, we used the model to explore the canopy scale photochemical pathways leading to VOC oxidation, radical production and ozone production. As illustrated in Figure 14, the strong attenuation of radiation resulted in an order of magnitude decrease in OH from the canopy top to the surface. Concurrently, NO_3 increased by a factor of 1.5 from the canopy top to the surface. For α,β-pinene these trends resulted in NO_3-initiated oxidation dominating α,β-pinene loss near the surface. The decrease in J-values also significantly reduced the importance of the $O(^1D) + H_2O$ channel for O_3 destruction to the point where α,β-pinene and β-caryophyllene ozonolysis reactions dominated O_3 destruction near the surface. Significant decreases in radical production rates near the surface were also simulated which resulted in net chemical O_3 destruction at the surface.

[30] We have also quantified the role of canopy scale photochemistry in modifying canopy top fluxes. Due to the extensive suite of measurements made during the CELTIC measurement intensive, the majority of the model input parameters were measured. The single parameter optimized to simulate the vertical mixing ratio profiles was the R factor in the eddy diffusivity parameterization as described in *Makar et al.* [1999]. Here we found an R factor of unity gave the best-fit to observations suggesting that near-field canopy effects were negligible for the Duke Forest site. This is in contrast to *Makar et al.* [1999] where an R = 0.15 was needed to simulate their observations at Borden, Ontario. The difference between these studies, given that we used the same modeling framework, indicates that near-field effects at the Duke Forest site could have been less important due to a different canopy structure or altered by the fumigation system operated during daytime. Typical σ_w and T_L values at Border were up to 0.8 m/s and 30–60 s compared to Duke Forest which had values for this intensive period of 0.4 m/s and 13 s, respectively. These differences result in considerably different length scales for near field effects ($\sigma_w \cdot T_L$) with estimates for Borden and Duke of 24–48 m and 6 m, respectively. Physically, the Borden site is spatially homogeneous, taller and has a more closely spaced canopy, while the Duke site is a more open Loblolly Pine canopy with much smaller fetch. Thus, the tower at Duke Forest may see significantly more aged isoprene. Future field programs should focus on a forest ecosystem with considerably larger fetch to compare with results from this study. A consequence of the Duke Forest canopy architecture is the more rapid venting of materials out of the canopy and a corresponding decrease in the residence time necessary for photochemistry to modify trace gas emissions.

[31] We conclude that the escape efficiency is a useful parameter to assess the impact of canopy-scale photochemistry on canopy top fluxes. We calculated an isoprene escape efficiency of 0.90 which is considerably larger than the value of 0.60 calculated by *Makar et al.* [1999]. Here, we also made an estimate for the β-caryophyllene escape efficiency of 0.30 for our base case assumptions. A series of urbanization scenarios showed that biogenic escape efficiencies were only moderately sensitive to anthropogenic pollution levels suggesting that a simple parameterization of escape efficiencies in regional air quality models in terms of grid cell NO_x mixing ratio may be possible.

[32] A sensitivity run with no β-caryophyllene emission resulted in nearly identical escape efficiencies for isoprene and α,β-pinene as the base case; however, the sensitivity run with β-caryophyllene emission at one order of magnitude larger than our base case did result in significant changes to the OH and O_3 fields, which will impact escape efficiency estimates for all biogenically emitted species. Future measurements of sesquiterpene basal emission rates are needed in order to quantify the importance of their oxidation products to secondary aerosol loading, and their potential impacts on atmospheric chemistry and climate.

[33] **Acknowledgments.** The Duke Forest site was supported by the Office of Science (BER), U.S. Department of Energy, grant DE-FG02-95ER62083. C.S. would like to thank NCAR's Advanced Study Program and the U.S. Environmental Protection Agency for funding. C.S. is appreciative of Barry Lefer and Rick Shetter for assistance in radiometer calibrations and Sasha Madronich for helpful discussions on canopy radiative transfer. The authors are also thankful to Ram Oren and Heather McCarthy for providing leaf area index data for the Duke Forest site.

References

Aschmann, S. M., J. Arey, and R. Atkinson (2002), OH radical formation from the gas-phase reactions of O_3 with a series of terpenes, *Atmos. Environ.*, *36*(27), 4347–4355.

Atkinson, R., and J. Arey (2003), Gas-phase tropospheric chemistry of biogenic volatile organic compounds: a review, *Atmos. Envron.*, *37*, suppl. 2., S197–S219

Barket, D. J., et al. (2004), A study of the NO_x dependence of isoprene oxidation, *J. Geophys. Res.*, *109*, D11310, doi:10.1029/2003JD003965.

Bey, I., B. Aumont, and G. Toupance (2001), A modeling study of the nighttime radical chemistry in the lower continental troposphere: 1. Development of a detailed chemical mechanism including nighttime chemistry, *J. Geophys. Res.*, *106*(D9), 9959–9990.

Chameides, W. L., R. W. Lindsay, J. Richardson, and C. S. Kiang (1988), The role of biogenic hydrocarbons in urban photochemical smog – Atlanta as a case study, *Science*, *241*(4872), 1473–1475.

Ciccioli, P., et al. (1999), Emission of reactive terpene compounds from orange orchards and their removal by within-canopy processes, *J. Geophys. Res.*, *104*(D7), 8077–8094.

Cleveland, C. C., and J. B. Yavitt (1997), Consumption of atmospheric isoprene in soil, *Geophys. Res. Lett.*, *24*, 2379–2382.

Di Carlo, P., et al. (2004), Missing OH reactivity in a forest: Evidence for unknown reactive biogenic VOCs, *Science*, *304*(5671), 722–725.

Doskey, P. V., and W. G. Gao (1999), Vertical mixing and chemistry of isoprene in the atmospheric boundary layer: Aircraft-based measurements and numerical modeling, *J. Geophys. Res.*, *104*(D17), 21,263–21,274.

Faloona, I., et al. (2001), Nighttime observations of anomalously high levels of hydroxyl radicals above a deciduous forest canopy, *J. Geophys. Res.*, *106*(D20), 24,315–24,333.

Fuentes, J. D., et al. (2000), Biogenic hydrocarbons in the atmospheric boundary layer: A review, *Bull. Am. Meteorol. Soc.*, *81*(7), 1537–1575.

Gao, W., M. L. Wesely, and P. V. Doskey (1993), Numerical modeling of the turbulent-diffusion and chemistry of NO_x, O_3, isoprene, and other reactive trace gases in and above a forest canopy, *J. Geophys. Res.*, *98*(D10), 18,339–18,353.

Griffin, R. J., D. R. Cocker, J. H. Seinfeld, and D. Dabdub (1999), Estimate of global atmospheric organic aerosol from oxidation of biogenic hydrocarbons, *Geophys. Res. Lett.*, *26*(17), 2721–2724.

Guenther, A. (1997), Seasonal and spatial variations in natural volatile organic compound emissions, *Ecol. Appl.*, *7*(1), 34–45.

Guenther, A. B., P. R. Zimmerman, P. C. Harley, R. K. Monson, and R. Fall (1993), Isoprene and monoterpene emission rate variability: Model evaluations and sensitivity analyses, *J. Geophys. Res.*, *98*(D7), 12,609–12,617.

Guenther, A., et al. (1995), A global model of natural volatile organic compound emissions, *J. Geophys. Res.*, *100*(D5), 8873–8892.

Guenther, A., B. Baugh, G. Brasseur, J. Greenberg, P. Harley, L. Klinger, D. Serca, and L. Vierling (1999), Isoprene emission estimates and uncertainties for the Central African EXPRESSO study domain, *J. Geophys. Res.*, *104*, 30,625–30,639.

Holzinger, R., A. Lee, K. T. Paw, and A. H. Goldstein (2004), Observations of oxidation products above a forest imply biogenic emissions of very reactive compounds, *Atmos. Chem. Phys. Discuss.*, *4*, 5345–5365.

Jacob, D. J. (2000), Heterogeneous chemistry and tropospheric ozone, *Atmos. Environ.*, *34*(12–14), 2131–2159.

Jacob, D. J., and S. C. Wofsy (1988), Photochemistry of biogenic emissions over the Amazon forest, *J. Geophys. Res.*, *93*, 1477–1486.

Jacobson, M. Z. (1999), *Fundamentals of Atmospheric Modeling*, Cambridge Univ. Press, New York.

Kanaya, Y., K. Nakamura, S. Kato, J. Matsumoto, H. Tanimoto, and H. Akimoto (2002), Nighttime variations in HO_2 radical mixing ratios at Rishiri Island observed with elevated monoterpene mixing ratios, *Atmos. Environ.*, *36*(31), 4929–4940.

Karl, T., M. Potosnak, A. Guenther, D. Clark, J. Walker, J. D. Herrick, and C. Geron (2004), Exchange processes of volatile organic compounds above a tropical rain forest: Implications for modeling tropospheric chemistry above dense vegetation, *J. Geophys. Res.*, *109*, D18306, doi:10.1029/2004JD004738.

Kurpius, M. R., and A. H. Goldstein (2003), Gas-phase chemistry dominates O_3 loss to a forest, implying a source of aerosols and hydroxyl radicals to the atmosphere, *Geophys. Res. Lett.*, *30*(7), 1371, doi:10.1029/2002GL016785.

Madronich, S., R. L. McKenzie, L. O. Bjorn, and M. M. Caldwell (1998), Changes in biologically active ultraviolet radiation reaching the Earth's surface, *J. Photochem. Photobiol. B, Biology*, *46*(1–3).

Makar, P. A., J. D. Fuentes, D. Wang, R. M. Staedler, and H. A. Wiebe (1999), Chemical processing of biogenic hydrocarbons within and above a temperate deciduous forest, *J. Geophys. Res.*, *104*(D3), 3581–3603.

Makar, P. A., M. D. Moran, M. T. Scholtz, and A. Taylor (2003), Speciation of volatile organic compound emissions for regional air quality modeling of particulate matter and ozone, *J. Geophys. Res.*, *108*(D2), 4041, doi:10.1029/2001JD000797.

Monson, R. K. (2002), Volatile organic compound emissions from terrestrial ecosystems: A primary biological control over atmospheric chemistry, *Isr. J. Chem.*, *42*(1), 29–42.

Monson, R. K., and E. A. Holland (2001), Biospheric trace gas fluxes and their control over tropospheric chemistry, *Ann. Rev. Ecol. Syst.*, *32*, 547+.

Paulson, S. E., M. Chung, A. D. Sen, and G. Orzechowska (1998), Measurement of OH radical formation from the reaction of ozone with several biogenic alkenes, *J. Geophys. Res.*, *103*(D19), 25,533–25,539.

Pierce, T., C. Geron, L. Bender, R. Dennis, G. Tonnesen, and A. Guenther (1998), Influence of increased isoprene emissions on regional ozone modeling, *J. Geophys. Res.*, *103*(D19), 25,611–25,629.

Raupach, M. R. (1988), Turbulent transfer in plant canopies, in *Plant Canopies—Their Growth, Form and Function*, edited by G. Russell, B. Marshall, and P. G. Jarvis, pp. 41–61, Cambridge Univ. Press, New York.

Raupach, M. R. (1989), A practical Lagrangian method for relating scalar concentrations to source distributions in vegetation canopies, *Q. J. R. Meteorol. Soc.*, *115*, 609–632.

Rottenberger, S., U. Kuhn, A. Wolf, G. Schebeske, S. T. Oliva, T. M. Tavares, and J. Kesselmeier (2004), Exchange of short-chain aldehydes between Amazonian vegetation and the atmosphere, *Ecol. Appl.*, *14*(4), suppl. S, S247–S262.

Shetter, R. E., et al. (2003), Photolysis frequency of NO_2: Measurement and modeling during the International Photolysis Frequency Measurement and Modeling Intercomparison (IPMMI), *J. Geophys. Res.*, *108*(D16), 8544, doi:10.1029/2002JD002932.

Sillman, S., et al. (2002), Loss of isoprene and sources of nighttime OH radicals at a rural site in the United States: Results from photochemical models, *J. Geophys. Res.*, *107*(D5), 4043, doi:10.1029/2001JD000449.

Stroud, C. A., et al. (2002), Nighttime isoprene trends at an urban forested site during the 1999 Southern Oxidant Study, *J. Geophys. Res.*, *107*(D16), 4291, doi:10.1029/2001JD000959.

Stroud, C. A., et al. (2004), Photochemistry in the arctic free troposphere: Ozone budget and its dependence on nitrogen oxides and the production rate of free radicals, *J. Atmos. Chem.*, *47*(2), 107–138.

Trainer, M., E. J. Williams, D. D. Parrish, M. P. Buhr, E. J. Allwine, H. H. Westberg, F. C. Fehsenfeld, and S. C. Liu (1987), Models and observations of the impact of natural hydrocarbons on rural ozone, *Nature*, *329*(6141), 705–707.

Wesely, M. L. (1989), Parameterization of surface resistances to gaseous dry deposition in regional-scale numerical models, *Atmos. Environ.*, *23*, 1293–1304.

Zaveri, R. A., C. M. Berkowitz, L. I. Kleinman, S. R. Springston, P. V. Doskey, W. A. Lonneman, and C. W. Spicer (2003), Ozone production efficiency and NO_x depletion in an urban plume: Interpretation of field observations and implications for evaluating O_3-NO_x-VOC sensitivity, *J. Geophys. Res.*, *108*(D14), 4436, doi:10.1029/2002JD003144.

B. Baker, South Dakota School of Mines and Technology, Rapid City, SD 57701, USA.

J. D. Fuentes, Department of Environmental Sciences, University of Virginia, Charlottesville, VA 22903, USA.

C. Geron, Environmental Protection Agency, Research Triangle Park, NC 27711, USA.

A. Guenther, T. Karl, and A. Turnipseed, National Center for Atmospheric Research, Boulder, CO 80307, USA.

P. Makar and C. Stroud, Meteorological Service of Canada, Toronto, Ontario, Canada M3H 5T4. (craig.stroud@ec.gc.ca)

E. Nemitz, Centre for Ecology and Hydrology, Edinburgh EH26 0QB, UK.

M. Potosnak, Desert Research Institute, Reno, NV 89512, USA.